Journal of Solid State Chemistry **146,** 439–447 (1999)
Article ID jssc.1999.8390, available online at http://www.idealibrary.com on IDEAL®

Thermal Stability of the Perovskite $BaBiO_3$

L. A. Klinkova,*,[1] V. I. Nikolaichik,† N. V. Barkovskii,* and V. K. Fedotov*

*Institute of Solid State Physics of the Russian Academy of Sciences (RAS), Moscow, Russia; and
†Institute of Microelectronics Technology and High Purity Materials of the RAS, Chernogolovka, Moscow District, 142432 Russia

Received March 9, 1999; accepted May 21, 1999

Thermal stability of the perovskite $BaBiO_3$ and phase relations in the $BaO–BiO_{1.5}(BiO_{2.5})$ system in the range of 45–55 mol%. $BiO_{1.5}$ at $p(O_2) = 0.21$ atm have been studied by thermogravimetric analysis, differential thermal analysis, X-ray diffraction, chemical analysis, and transmission electron microscopy. It has been found that $BaBiO_3$ loses oxygen in the temperature range between 600 and 1015°C with formation of the oxygen-deficient phases $BaBiO_{2.88}$, $BaBiO_{2.83}$, $BaBiO_{2.75}$, and $BaBiO_{2.55}$. $BaBiO_3$ and the oxygen-deficient phases form two-phase regions involving phases of the perovskite series $Ba_mBi_{m+n}O_y$ at the Bi-rich side and $Ba_{m+n}Bi_mO_y$ at the Ba-rich side. At 1015°C the $BaBiO_{2.55}$ phase exhibits incongruent melting. At further increasing temperature the 1:1 (Ba:Bi) sample passes through a sequence of the crystallization fields of the Ba-rich phases of the compositions 5:4, 4:3, 3:2, 9:5, and 17:9, reaching the complete melting state at 1100°C. © 1999 Academic Press

1. INTRODUCTION

The phenomenon of superconductivity in the Ba–Pb–Bi–O (1) and K–Ba–Bi–O (2) systems generates interest in studying of the parent system Ba–Bi–O. This system comprises the perovskite $BaBiO_3$ containing bismuth ions of different oxidation states (+3 and +5) (3) in an ordered arrangement (4, 5), which gives rise to a charge density wave being responsible for the semiconducting behavior of $BaBiO_3$ (6, 7).

After heating to ≈600°C in air, $BaBiO_3$ with monoclinic structure at room temperature undergoes phase transformations to rhombohedral (130°C) and cubic (475–530°C) structures without noticeable change of oxygen content (8). Upon further heating, a visible loss of oxygen is observed.

Thermogravimetric studies (9, 10) show that oxygen loss proceeds in three quasistationary stages, the extent thereof being dependent on oxygen pressure. The maximally depleted oxygen state $BaBiO_{2.5}$ was reported to exist was in a perovskite structure (9, 11) and in a layered nonperovskite structure (12). Different points of view regarding the phase composition, which takes place in the conversion of $BaBiO_3$ into $BaBiO_{2.5}$, have been argued. Those include proposals that oxygen loss begins with the formation of three phases (9) $BaBiO_{3-x}$ ($0 < x \leq 0.03$), $BaBiO_{2.80}$ (or $BaBiO_{2.82}$ according to (13)), and $BaBiO_{2.55}$, of two phases $BaBiO_{2.97}$ and $BaBiO_{2.77}$ (14), of three phases of nondeclared compositions (15), and of one oxygen-deficient phase of variable composition $BaBiO_{3-x}$ (11). The formation of discrete phases $BaBiO_{2.88}$, $BaBiO_{2.83}$, $BaBiO_{2.75}$, and $BaBiO_{2.52}$ has been revealed in (16) upon oxygen removal from $BaBiO_3$ samples using both argon annealing and electron irradiation in a transmission electron microscope.

In this work, we have attempted to establish whether the phases found in (16) exist in air ($p(O_2) = 0.21$ atm) and what is the character of phase relations in the $BaO–BiO_{1.5}$ ($BiO_{2.5}$) system in the 45–55 mol% $BiO_{1.5}$ range with the ratio Ba:Bi = 1:1; to carry this out we used thermogravimetric (TG), differential thermal analysis (DTA), X-ray diffraction (XRD), chemical analysis, electron diffraction, and elemental analysis in a transmission electron microscope (TEM).

2. EXPERIMENTAL

TG and DTA were performed in Al_2O_3 crucibles with a Q1500D Derivatograph at a heating rate of 900°C/h. Samples for DTA were prepared by sintering homogenized and compacted mixtures of BaO_2 (analytical grade) or $Ba(NO_3)_2$ (reagent grade) and Bi_2O_3 (reagent grade) with a step of 0.25–0.5 mol% $BiO_{1.5}$. Sintering was performed in Al_2O_3 crucibles at 900–1000°C for 24 h, after that the samples were slowly cooled (20°C/h) to room temperature.

Samples for chemical analysis, XRD, and TEM studies were synthesized by two procedures: ceramic and molten. In the first procedure, the starting mixture was heated in air first at 600°C for 24 h, followed by annealing at specified temperatures. Intermediate homogenization of samples was used in several cases. Molten samples were produced by

[1] To whom correspondence should be addressed. E-mail: klinkova@issp.ac.ru.

0022-4596/99 $30.00

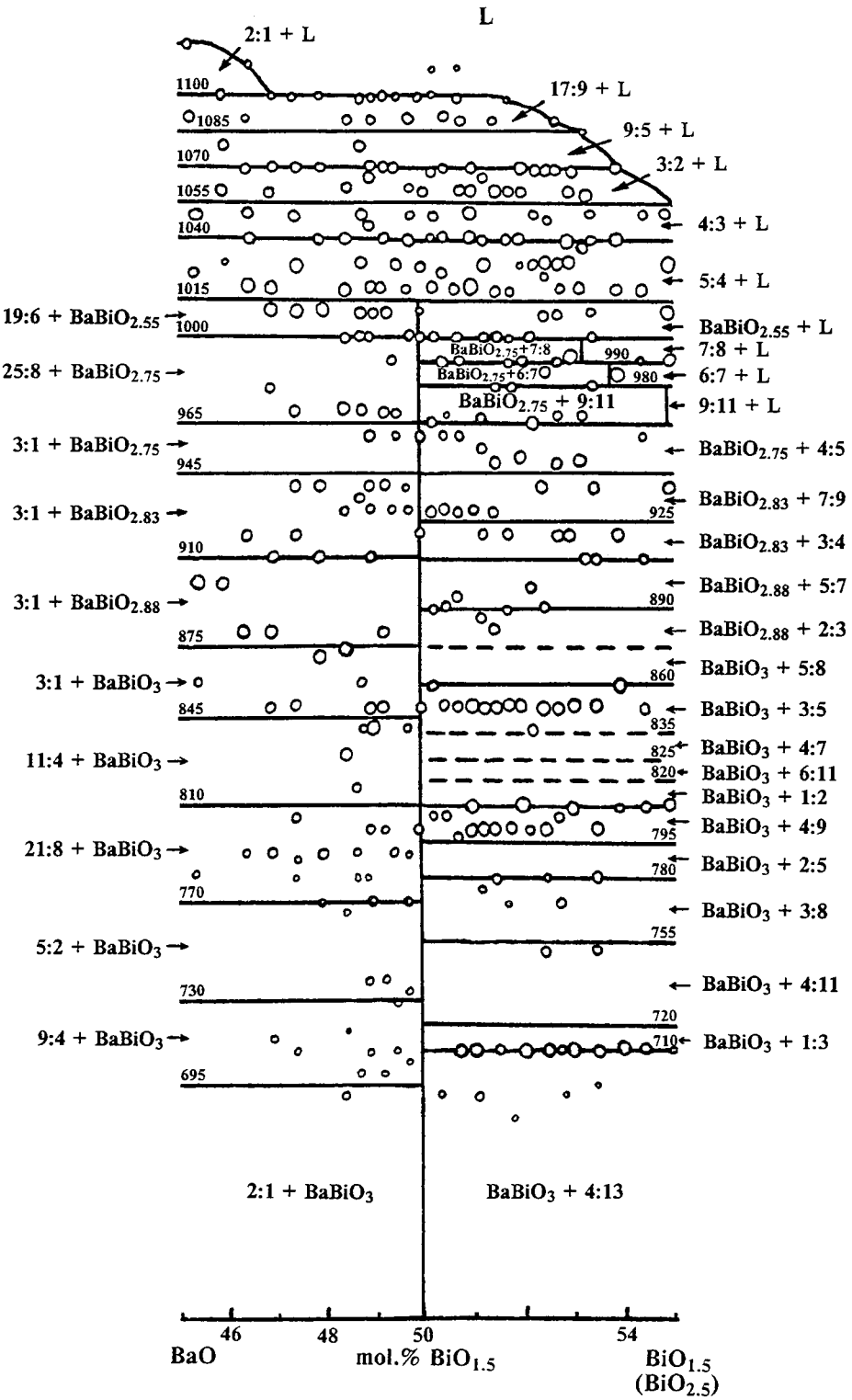

FIG. 1. The phase diagram of the Bao–$BiO_{1.5}$($BiO_{2.5}$) system around the 1:1 (Ba:Bi) composition at $p(O_2) = 0.21$ atm mapped out on the basis of DTA data.

heating starting tablets with rising temperature for 2–3 h until the tablets were completely melted. After being kept at the final temperature for 0.5–1 h for homogenization, the melt was rapidly cooled (to avoid an intensive interaction with the crucible) to solidus temperature followed by cooling at a rate of 30–60°C/h. Phase composition of the sam-

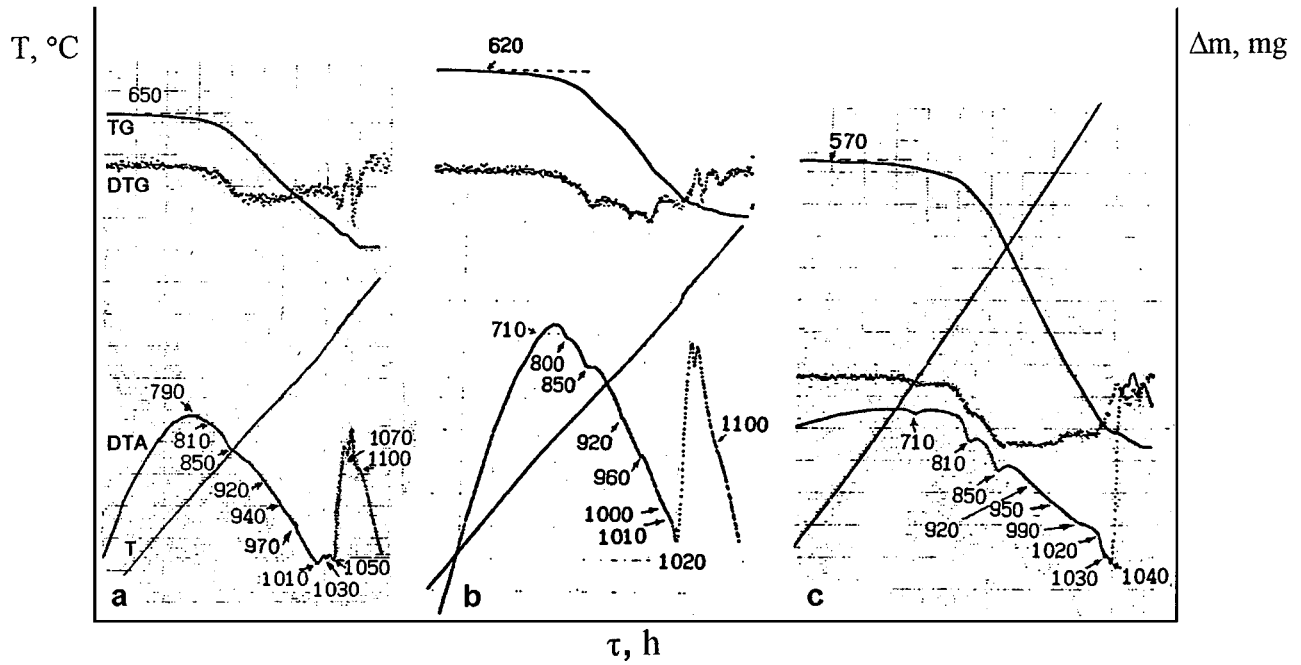

FIG. 2. T, TG, DTG, and DTA heating curves for samples of (a) 47.5 mol% $BiO_{1.5}$ ($m = 0.7887$ g), (b) 50 mol% ($m = 0.9002$ g), and (c) 52 mol% ($m = 1.9538$ g).

ples was analyzed at intermediate temperatures by quenching them in liquid nitrogen.

Samples for XRD were ground under vaseline layer for protection against air. X-ray diffraction patterns were obtained on a D-500 Siemens diffractometer at room temperature. Samples for a JEM-2000FX transmission electron microscope equipped with an AN10/95S analytical system were ground and applied in the form of suspension onto thin carbon films.

The average oxidation state of bismuth $\bar{B}i$, which was also used for calculation of the oxygen index (y), was determined by iodometric titration. An absolute error in the determination of $\bar{B}i$ did not exceed ± 0.02.

3. RESULTS

Figure 1 shows the diagram of phase relations in the system $BaO–BiO_{1.5}(BiO_{2.5})$ near the 1:1 composition at $p(O_2) = 0.21$ atm mapped out in accordance with the effects (peaks) on the heating DTA curves. The examples of the curves are given in Fig. 2. The size of the circle in Fig. 1 is conventionally related with magnitude of the corresponding peak. The temperatures of phase boundaries in Fig. 1 are, in fact, somewhat tentative ($\Delta \approx 10^\circ$C), since positions of the peaks depend on the heating rate and weight of the DTA samples. The existence of the phase boundaries is pronounced if one traces them in the broader composition ranges of 20–50 (17) and 50–80 mol% $BiO_{1.5}$ (18).

It is seen from Fig. 2 that samples lose oxygen (TG curves) from $\approx 600^\circ$C to the point of complete melting with peaks in the rate loss (DTG curves) that agree with the peaks on the DTA curves. $BaBiO_y$ ceramic samples produced by annealing at 800, 900, 950, and 1000°C have oxygen index values of 3.00, 2.85, 2.75, and 2.65, respectively, in agreement with the values reported in (11).

X-ray diffraction patterns of the 1:1 samples annealed at 800, 900, 950, and 1000°C (Fig. 3) look similar to those given in (11). Comparison of X-ray patterns in Fig. 3 with those in (16) shows that the same oxygen-deficient phases are present in the samples annealed in air and in argon. This conclusion was also supported by the observation of individual particles in the TEM, showing that the samples contain different oxygen-deficient phases, which were clearly distinguished by electron diffraction patterns. The phases $BaBiO_{2.88}$, $BaBiO_{2.83}$, and $BaBiO_{2.75}$ are of ordered perovskite structures, which give rise to the characteristic types of supercell reflections (Fig. 4). Table 1 presents data on observations of particles found in the samples. The data obtained with the TEM procedure can be used for the estimation of phase percentages. However, quantitative phase percentages are difficult to determine from the TEM data as they are subject to statistical selection. There is also a crucial challenge in discriminating the percentages of the $BaBiO_3$ and $BaBiO_{2.88}$ phases in particles displaying supercell reflections characteristic of the latter phase. These particles may have a domain structure formed of $BaBiO_3$ and

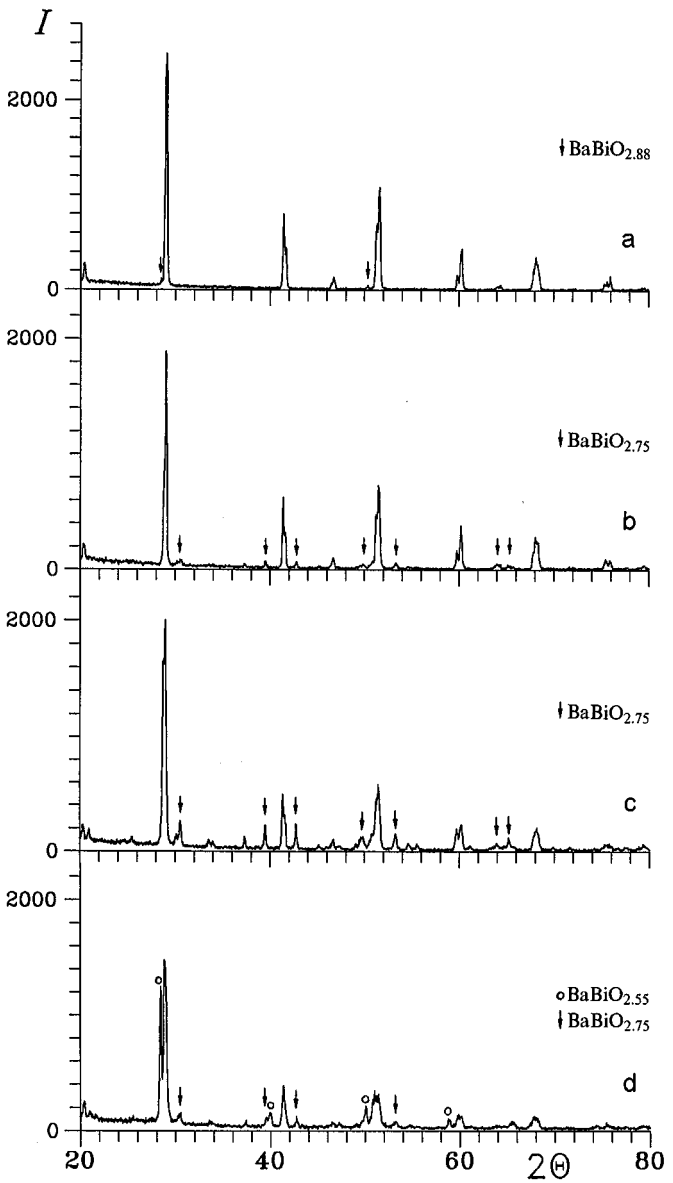

FIG. 3. X-ray powder patterns of the 1:1 samples annealed at (a) 800, (b) 900, (c) 950, and (d) 1000°C in air. Some specific peaks of the phases are shown.

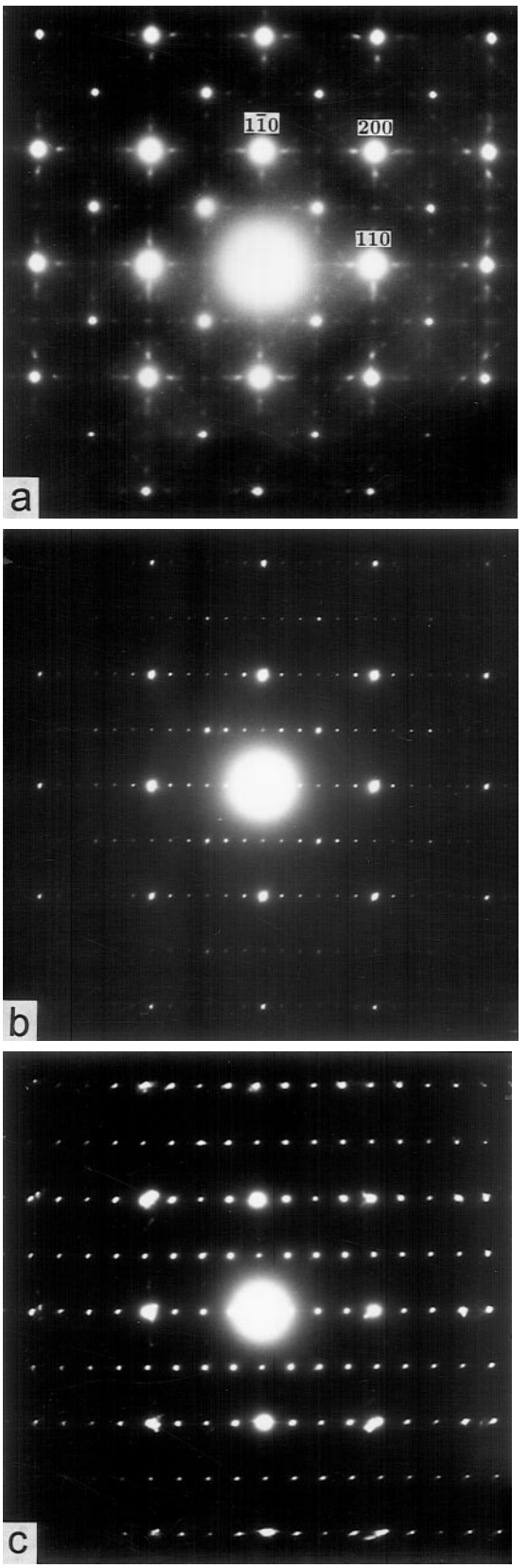

FIG. 4. Electron diffraction patterns ([001] zone axis) of the oxygen-deficient phases (a) $BaBiO_{2.88}$, (b) $BaBiO_{2.83}$, and (c) $BaBiO_{2.75}$.

$BaBiO_{2.88}$, as is evident from the data in the Table 1, which shows that the oxygen index is close to 3 at 800°C, whereas a significant fraction of the particles display diffraction patterns with the supercell spots arising from thin domains of $BaBiO_{2.88}$. It is apparent that a small oxygen loss starting at 600°C (Fig. 2) is associated with the $BaBiO_{2.88}$ phase, and the greatest fraction of oxygen-deficient phases existing at 950°C stems from $BaBiO_{2.75}$. It should be noted that $BaBiO_3$ persists in the samples up to 1000°C.

$BaBiO_3$ and the oxygen-deficient phases form a series of two-phase regions with perovskite phases $Ba_mBi_{m+n}O_y$ at

TABLE 1
Chemical Analysis and TEM Studies of $BaBiO_y$ Ceramic Samples

1		2	3	4	5			
T, °C	time, h				$BaBiO_3$	$BaBiO_{2.88}$	$BaBiO_{2.83}$	$BaBiO_{2.75}$
800	48	3.00	4.00	30	63	37		
900	96	2.85	3.70	30	34	33	3	30
950	72	2.75	3.50	28	10	11		79

Note. 1, annealing condition; 2, oxygen index (y); 3, the average oxidation state of bismuth; 4, number of investigated particles; 5, percentage (%) of particles displaying diffraction patterns with the characteristic supercell spots of the phases.

the Bi-rich side (Fig. 1). The presence of $Ba_mBi_{m+n}O_y$ phases is detected by XRD (Fig. 5) and TEM studies of Bi-rich samples (Table 2), although X-ray identification of the cubic phase 4:13 in samples of compositions near 50 mol% $BiO_{1.5}$ may be difficult, as the peak positions of the 4:13 phase marked in Fig. 5b are very close to the positions of some peaks of $BaBiO_3$. The composition of the $Ba_mBi_{m+n}O_y$ phases changes with temperature in accordance with the disposition of these phases in the liquidus–solidus region (20). All the $Ba_mBi_{m+n}O_y$ phases are of ordered structures giving rise to the characteristic pictures of supercell spots in electron diffraction patterns (Fig. 6a).

Phase equilibria in the samples is evidenced by consistency of the phase composition irrespective of whether the equilibrium was reached by "upward" or "downward" heating direction and without regard to the difference in the morphology (tablets and boules) of the samples in ceramic and molten procedures. That the equilibrium in the system is rapidly reached is also attested by satisfactory agreement of values of oxygen loss in DTA samples continuously heated at a rate of 900°C/h and in samples quenched at isothermal annealing. Some samples demonstrate the occurrence of several $Ba_{m+n}Bi_mO_y$ phases simultaneously, which may be due to the temperature gradient (≈ 10°C) comparable with a 10–20°C width of the two-phase regions. The obtained data show the absence of a cation homogeneity region from $BaBiO_3$ toward Bi_2O_3 that is in contrast with (22), which advocates a wide region extending up to 62.1 mol% $BiO_{1.5}$.

The 1:1 phases form two-phase regions with $B_{m+n}B_mO_y$ phases at the Ba-rich side of the phase diagram (Fig. 1). The $Ba_{m+n}Bi_mO_y$ phases are also of ordered perovskite structures (17). Characteristic electron diffraction patterns of the $Ba_{m+n}Bi_mO_y$ phases can be observed on particles present in samples of compositions close to the $(m+n):m$ ratio. In contradiction to 1:1 and Bi-rich samples, where phase separation is identified at least by the TEM procedure (the sizes of investigated particles can be less than one μm), the specific feature of oxide materials in the 46–50 mol% $BiO_{1.5}$ region has been observed.

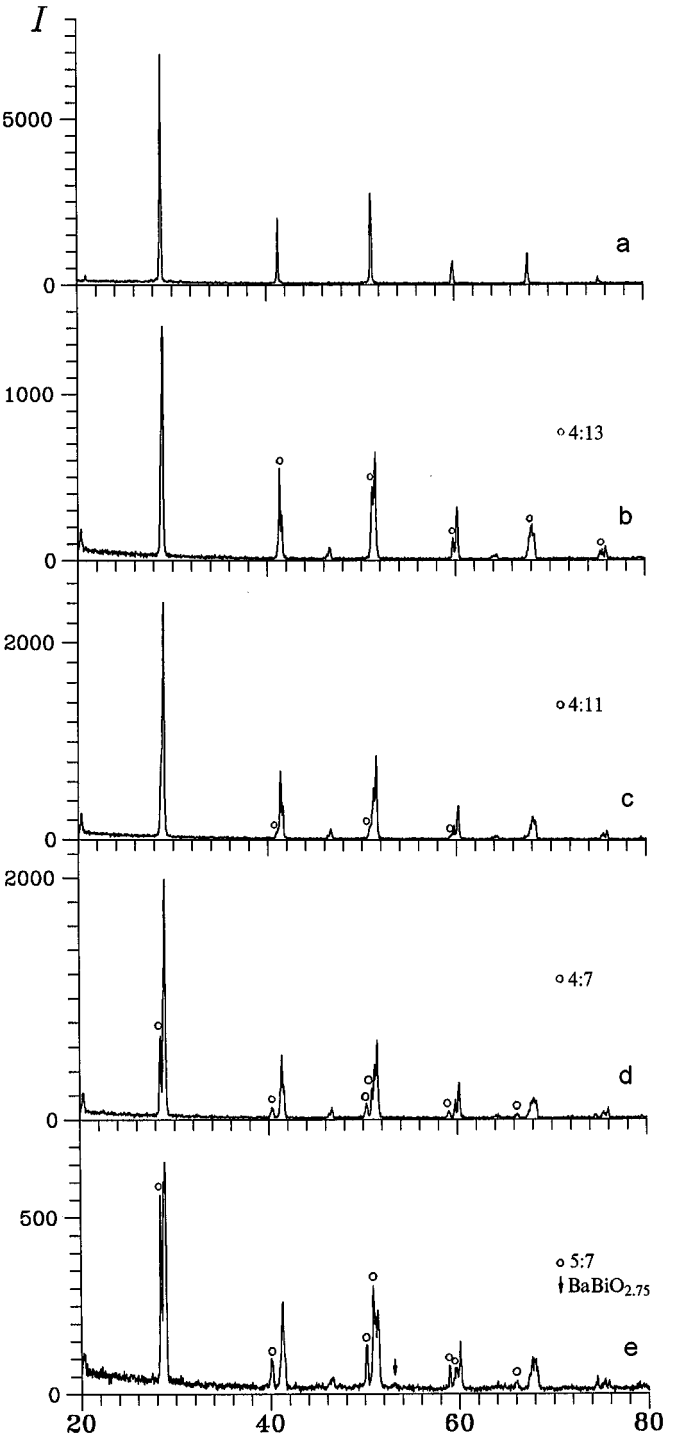

FIG. 5. X-ray powder patterns of the 4:13 sample cooled down to room temperature (a) and 52 mol% $BiO_{1.5}$ samples quenched at (b) 600, (c) 750, (d) 830, and (e) 900°C.

TABLE 2
Chemical Analysis and TEM Studies of 51 mol% $BiO_{1.5}$ Samples

1		2	3										
T, °C	time, h		6:7	9:11	4:5	7:9	3:4	2:3	4:7	1:2	2:5	4:11	1:3	4:13
20[a]		3.98												+
600[b]	24	3.86												+
600[c]	24	3.96												+
700[b]	1	3.88											+	
700[c]	24	3.96											+	
750[a]	1	3.94									+	+		
800[c]	1	3.98							+	+				
850[a]	1	3.72			+	+								
850[b]	0.5	3.66				+	+	+						
900[a]	1	3.52			+									
900[b]	0.5	3.48			+									
920[b]	0.5	3.36			+									
940[b]	0.5	3.22			+									
950[a]	1	3.28												
950[c]	284	340			+									
980[b]	0.5	3.20	+	+	+									
1000[b]	0.5	3.10	+	+	+									
1010[c]	0.5	3.10	+	+	+									
1020[b]	0.5	3.06												

Note. 1, preparation condition: [a] cooling from the melting temperature (1050°C), [b] ceramic synthesis, [c] reverse heating after synthesis by the molten procedure; 2, the average oxidation state of bismuth; 3, particles of the $Ba_mBi_{m+n}O_y$ phases found in the samples (TEM data for 950[a] and 1020[b] are not available).

It is found that samples from the two-phase Ba-rich regions do contain particles of the oxygen-deficient phases, but percentages of particles displaying electron diffraction patterns thereof are small (Table 3). Electron diffraction patterns of the greatest fraction of particles do not show (Fig. 6b) supercell spots characteristic of neither the oxygen-deficient phases nor the $Ba_{m+n}Bi_mO_y$ phases. Most of the particles of a Ba-rich material cooled to low temperatures ($< \approx 850$°C) display diffraction patterns with the $\frac{1}{2}[111]$-type spots (shown by the arrow in Fig. 6c). Particles of a material quenched at high temperature tend to give rise to only strong ($h + k + l = 2n$) and weak ($h + k + l = 2n + 1$) perovskite spots. The presence or the absence of the $\frac{1}{2}[111]$-type spots result in different X-ray or neutron characterization. A material displaying the $\frac{1}{2}[111]$-type spots can be ascribed as having a distorted perovskite structure (e.g., of the space group $I2/m$ $R3m$, or $Fm3m$), the other material as having the nondistorted cubic structure of the $Pm3m$ group. Figure 7a presents the X-ray diffraction profile of $BaBiO_3$ having the $I2/m$ monoclinic structure at room temperature which may be compared with X-ray profiles in Figs. 7b and 7c corresponding to materials with a distorted noncubic structure of a higher symmetry. The profile in Fig. 7d corresponds to a material consisting mostly of cubic phases. One is inclined to suggest that Ba-rich materials not displaying supercell spots in electron diffraction patterns are formed of disorientated domains of $Ba_{m+n}Bi_mO_y$, and that the 1:1 phases of several nm in size are not enough to realize diffraction conditions for the appearance of the supercell reflections.

In the 1000–1015°C temperature region, the tetragonal phase $BaBiO_{2.55}$ with cell parameters $a = 4.362$, $b = 4.509$ Å (Fig. 8a) exists and has a crystallization field of its own. According to the phase diagram (Fig. 1), the $BaBiO_{2.55}$ phase begins to melt incongruently at 1015°C, then the 1:1 sample goes through the crystallization fields of phases 5:4, 4:3, 3:2, 9:5, and 17:9, where the average oxidation state of bismuth is 3.02–3.06. The samples quenched in these crystallization fields comprise two phases, one of the crystallizing phases is a Ba-rich phase, the composition of other phase corresponds to that of Bi-rich liquid (Fig. 8b). According to the DTA data (Fig. 2) the last weak endothermal effect takes place at 1100°C.

A higher degree of oxygen deficiency of 1:1 samples can be achieved at annealing in atmosphere with a low oxygen partial pressure. The orthorhombic phase $BaBiO_{2.52}$ (Fig. 9a) with cell parameters $a = 4.397$, $b = 4.389$, $c = 4.493$ Å can be formed with annealing in argon (1000°C, 24 h). X-ray diffraction patterns of the $BaBiO_{2.55}$ and $BaBiO_{2.52}$ phases are similar to those of the $Ba_mBi_{m+n}O_y$ phases, which were considered by Aurivillius (19) as $Ba_xBi_{1-x}O_y$ phases with solid solution structure. We were not able to obtain electron

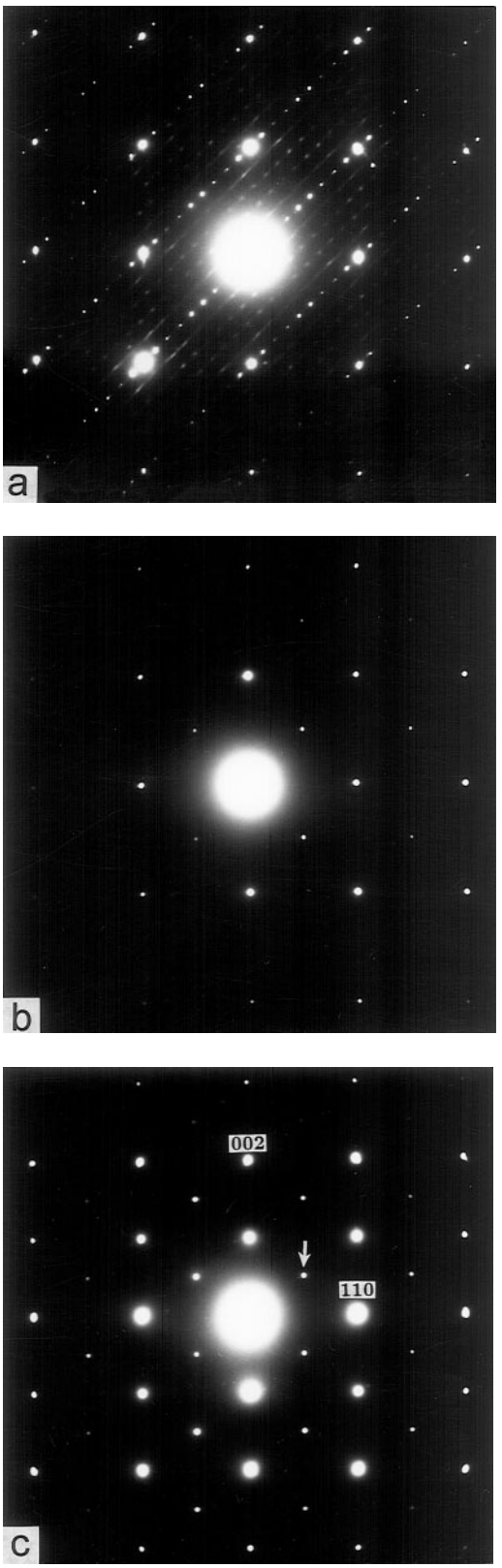

FIG. 6. Electron diffraction patterns of the Bi-rich phase of the composition (a) 4:5 and a Ba-rich material in the (b) [100] and (c) [$1\bar{1}0$] zone axis.

TABLE 3
Chemical Analysis and TEM Studies of 48 mol% $BiO_{1.5}$ Ceramic Samples

1		2	3	4		
T, °C	time, h			$BaBiO_{2.88}$	$BaBiO_{2.83}$	$BaBiO_{2.75}$
820	1	4.00	50	5		
900	1	3.63	57		5	11
950	20	3.40	40		3	10

Note. 1, annealing condition; 2, the average oxidation state of bismuth; 3, number of investigated particles; 4, percentage (%) of particles displaying diffraction patterns with the characteristic supercell spots of the oxygen-deficient phases.

diffraction patterns of the $BaBiO_{2.55}$ and $BaBiO_{2.52}$ phases (because of samples degradation in air) to find if these phases have ordered structures.

The $BaBiO_{2.5}$ phase with the nonperovskite structure (Fig. 9b) of the space group $P2_1/c$ (12) most likely lacks the crystallization field at $p(O_2) = 0.21$ atm. This phase, containing no Bi^{5+} ions, was synthesized by annealing $BaBiO_3$ under the dynamic vacuum conditions (750°C, 17 h). The lattice parameters of the $BaBiO_{2.5}$ phase were determined to be $a = 7.336$, $b = 7.583$, $c = 6.076$ Å, $\beta = 99.20°$.

4. DISCUSSION

The $BaBiO_{3-x}$ system is an oxygen-open system when equilibrium is established at higher temperature with the corresponding oxygen loss. Oxygen loss occurs with the formation of oxygen-deficient phases $BaBiO_{2.88}$, $BaBiO_{2.83}$, $BaBiO_{2.75}$, and $BaBiO_{2.55}$. The heterogeneous equilibrium in the system can be described with the general reaction $BaBiO_3(s) = BaBiO_{3-x}(s) + x/2O_2(g)$ including the stages of conversion of $BaBiO_3$ into oxygen-deficient phases:

$$BaBiO_3 = BaBiO_{2.88} + 0.06O_2 \quad [1]$$

$$BaBiO_3 = BaBiO_{2.83} + 0.085O_2 \quad [2]$$

$$BaBiO_3 = BaBiO_{2.75} + 0.125O_2 \quad [3]$$

$$BaBiO_3 = BaBiO_{2.55} + 0.225O_2. \quad [4]$$

The equilibrium established through reactions [1–4] depends on oxygen pressure. At $p(O_2) = 0.21$ atm, reactions [1–3] are displaced to the left so that the products coexist with $BaBiO_3$ persisting up to 1000°C. Reaction [4] is displaced to the right.

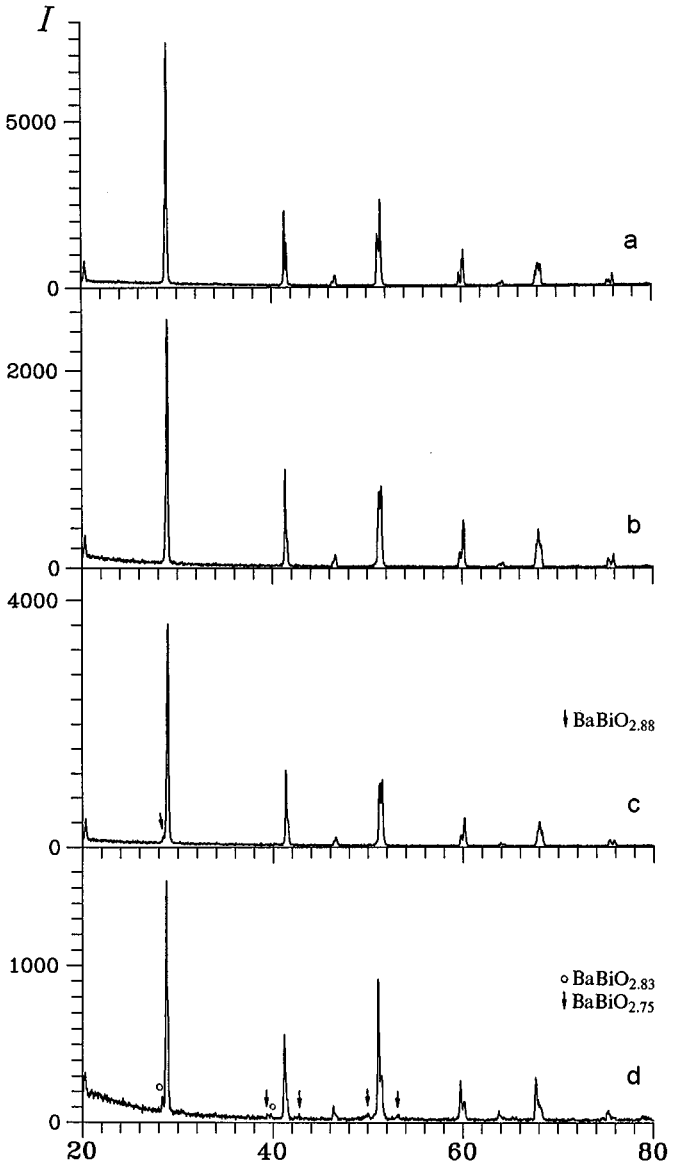

FIG. 7. X-ray powder patterns of the 1:1 sample cooled down to room temperature (a) and 48 mol% $BiO_{1.5}$ samples quenched at (b) 750, (c) 820, and (d) 900°C.

If one supposes that oxygen loss proceeds in the sequential stages:

$$BaBiO_3 = BaBiO_{2.88} + 0.06O_2 \quad [5]$$

$$BaBiO_{2.88} = BaBiO_{2.83} + 0.025O_2 \quad [6]$$

$$BaBiO_{2.83} = BaBiO_{2.75} + 0.04O_2 \quad [7]$$

$$BaBiO_{2.75} = BaBiO_{2.55} + 0.1O_2 \quad [8]$$

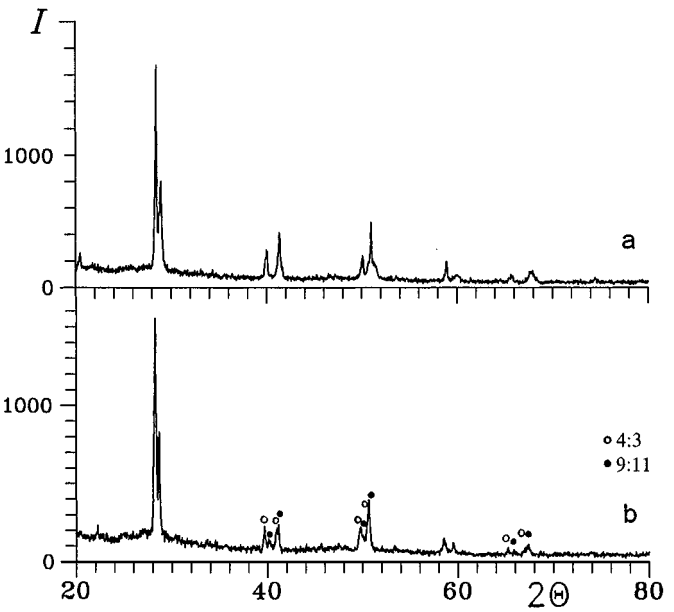

FIG. 8. X-ray powder patterns of the 1:1 samples annealed at (a) 1010 and (b) 1050°C in air.

which are observed in small particles irradiated in the column of electron microscope at $p(O_2) \sim 10^{-9}$ atm (16), the existence of $BaBiO_3$ in samples throughout the 600–1000°C range at $p(O_2) = 0.21$ atm cannot be explained.

Simultaneous presence of the products of the reactions is also assisted by the isostructural similarity of the phases

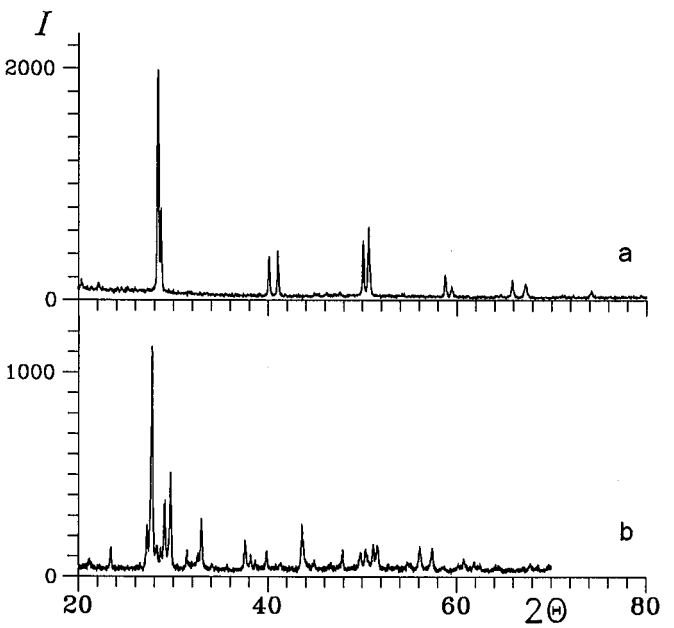

FIG. 9. X-ray powder patterns of the 1:1 samples annealed in (a) argon (1000°C, 24 h) and (b) under dynamical vacuum (750°C, 17 h).

that permits coherent intergrowth of domains of the phase, making oxygen outflow more difficult. It results to the capsulation effect when surface layers formed of phases with lower oxygen content insulate the bulk interior with higher oxygen content. This assumption was earlier argued in (15), where oxygen-deficient materials were studied both by X-rays penetrating only into surface layers (several μm) and by neutrons sampling the whole volume.

The multiphase state of 1:1 samples as well as samples of other compositions being synthesized provides enough reason to consider the diagram in Fig. 1 as an idealized one since it is representative of the compositions of dominant phases in the samples.

The crystallization region of the phase diagram of the $BaO–BiO_{1.5}(BiO_{2.5})$ system mapped out on the basis of DTA data is somewhat different from that of in the 30–55.5 mol% $BiO_{1.5}$ range constructed on the basis of visual polythermal analysis (VPA) data (21). In the latter diagram, a 1:1 sample melts congruently at 1065°C and forms feebly marked eutectics with the Bi-rich (7:8) and the Ba-rich (5:4) phases. The variation in the DTA and VPA versions of the crystallization regions may be attributed to a limited potential of the VPA to register the state of complete melting.

4. CONCLUSIONS

This study supports the fact of complex transformations observed at heating $BaBiO_3$ (9–11). It shows that oxygen loss in air results in the formation of four oxygen-deficient phases $BaBiO_{2.88}$, $BaBiO_{2.83}$, $BaBiO_{2.75}$, and $BaBiO_{2.55}$. The phases can coexist simultaneously in samples, at increasing temperature the ratio of these phases changes so that one of them is dominant in a temperature range between 600 and 1015°C. $BaBiO_3$ and the oxygen-deficient phases form two-phase regions with discrete Ba-rich and B-rich perovskite phases. The $BaBiO_{2.55}$ phase melts incongruently at 1015°C leading to the formation of the Ba-rich (5:4) solid and a Bi-rich liquid. At further heating the 1:1 sample goes through crystallization fields of other Ba-rich phases of compositions 4:3, 3:2, 9:5, and 17:9 reaching the complete melting state at 1100°C.

ACKNOWLEDGMENTS

This work was supported by the Superconductivity Division of the State Scientific and Technical Program "Actual Problems of Condensed Matter Physics" (Project Volna-4) and of the Russian Foundation for Basic Research (Project 99-02-16117).

REFERENCES

1. A. W. Sleight, J. L. Gillson, and P. E. Bierstedt, *Solid State Commun.* **17,** 27 (1975).
2. L. F. Mattheis, E. M. Gyorgy, and D. W. Johnson, *Phys. Rev. B* **37,** 3745 (1988).
3. V. R. Scholder, K.-W. Ganter, H. Glasser, and G. Merz, *Z. Anorg. Allg. Chem.* **319,** 375 (1963).
4. D. E. Cox and A. W. Sleight, *Solid State Commun.* **19,** 969 (1976).
5. G. Thornton and A. J. Jacobson, *Acta Crystallogr. Sect. B* **34,** 351 (1978).
6. T. Nakamura, S. Kose, and T. Sata, *J. Phys. Soc. Japan* **31,** 1284 (1971).
7. L. F. Mattheis and D. R. Hamann, *Phys. Rev. B* **28,** 422 (1983).
8. D. E. Cox and A. W. Sleight, *Acta Crystallogr. Sect. B* **35,** 1 (1979).
9. R. A. Beyerlein, A. J. Jacobson, and L. N. Yacullo, *Mater. Res. Bull.* **20,** 877 (1985).
10. Y. Saito, T. Maruayama, and A. Yamanaka, *Thermochim. Acta.* **115,** 199 (1987).
11. F. Abbattista, M. Valino, A. Delmastro, D. Mazza, and S. Ronchetti, *J. Solid State Chem.* **11,** 55 (1995).
12. P. Lightfoot, J. A. Hriljack, S. Pei, Y. Zheng, A. W. Mitchell, D. R. Richards, B. Dabrowski, J. D. Jorgensen, and D. G. Hinks, *J. Solid State Chem.* **92,** 473 (1991).
13. S. Pei, J. D. Jorgensen, D. G. Hinks, P. Lightfoot, Y. Zheng, D. R. Richards, B. Dabrowski, and A. W. Mitchell, *Mater. Res. Bull.* **25,** 1467 (1990).
14. C. Chaillout and J. P. Remeika, *Solid State Commun.* **5,** 833 (1985).
15. H. Kusuhara, A. Yamanaka, H. Sakuma, and H. Hashizume, *Jpn. J. Appl. Phys.* **28,** 678 (1989).
16. L. A. Klinkova, V. I. Nikolaichik, N. V. Barkovskii, and V. K. Fedotov, *Rus. J. Inorg. Chem.* **42,** 810 (1997).
17. L. A. Klinkova, V. I. Nikolaichik, N. V. Barkovskii, and V. K. Fedotov, *Russ. Chem. Bull.*, submitted.
18. L. A. Klinkova, V. I. Nikolaichik, N. V. Barkovskii, and V. K. Fedotov, *Rus. J. Inorg. Chem.*, submitted.
19. B. Aurivillius, *Arkiv Kemi. Min. Geol.* **16A,** 17 (1943).
20. L. A. Klinkova, V. I. Nikolaichik, L. V. Zorina, N. V. Barkovskii, V. K. Fedotov, and S. A. Zver'kov, *Rus. J. Inorg. Chem.* **41,** 683 (1996).
21. L. A. Klinkova, V. I. Nikolaichik, N. V. Barkovskii, and V. K. Fedotov, *Rus. J. Inorg. Chem.* **42,** 1416 (1997).
22. A. V. Shevchuk, "3rd All-Union conference on physical-chemical basis of technology of ferroelectrics and related compounds. Zvenigorod, 1988," p. 56. [Abstract]